We are IntechOpen, the world's leading publisher of Open Access books Built by scientists, for scientists

6,900
Open access books available

185,000
International authors and editors

200M
Downloads

154
Countries delivered to

Our authors are among the

TOP 1%
most cited scientists

12.2%
Contributors from top 500 universities

BOOK CITATION INDEX
CLARIVATE ANALYTICS
INDEXED

WEB OF SCIENCE™

Selection of our books indexed in the Book Citation Index
in Web of Science™ Core Collection (BKCI)

Interested in publishing with us?
Contact book.department@intechopen.com

Fluid Flow and Heat Transfer Analyses in Curvilinear Microchannels

Sajjad Bigham[1] and Maryam Pourhasanzadeh[2]
[1]School of Mechanical Engineering, College of Engineering, University of Tehran,
[2]School of Mechanical Engineering, Power and Water University of Technology,
[1,2]Iran

1. Introduction

Due to the wide application of curvy channels in industrial systems, various analytical, experimental and numerical works have been conducted for macro scale channels in curvilinear coordinate. Cheng [8] studied a family of locally constricted channels and in each case, the shear stress at the wall was found to be sharply increased at and near the region of constriction. O'Brien and Sparrow [9] studied the heat transfer characteristics in the fully developed region of a periodic channel in the Reynolds number range of Re=1500 to Re=25000. A level of heat transfer enhancement by about a factor of 2.5 over a conventional straight channel was observed, resulting from a highly complex flow pattern including a strong forward flow and an oppositely directed recalculating flow. Nishimura et al. [10] numerically and experimentally investigated flow characteristics in a channel with a symmetric wavy wall. They obtained the relationship between friction factor and Reynolds number. Also, they found that in the laminar flow range, the friction factor is inversely proportional to Reynolds number. Furthermore, there is small peak in the friction factor curve which was accredited to the flow transition. The numerical prediction of the pressure drop was in good agreement with the measured values until about Re= 350. Wang et al. [11] numerically studied forced convection in a symmetric wavy wall macro channel. Their results showed that the amplitudes of the Nusselt number and the skin-friction coefficient increase with an increase in the Reynolds number and the amplitude–wavelength ratio. The heat transfer enhancement is not significant at smaller amplitude wavelength ratio; however, at a sufficiently larger value of amplitude wavelength ratio the corrugated channel will be seen to be an effective heat transfer device, especially at higher Reynolds numbers.

Also in microscale gas flows, various analytical, experimental and numerical works have been conducted. Arkilic et al. [12] investigated helium flow through microchannels. It is found that the pressure drop over the channel length was less than the continuum flow results. The friction coefficient was only about 40% of the theoretical values. Beskok et al. [13] studied the rarefaction and compressibility effects in gas microflows in the slip flow regime and for the Knudsen number below 0.3. Their formulation is based on the classical Maxwell/Smoluchowski boundary conditions that allow partial slip at the wall. It was

shown that rarefaction negates compressibility. They also suggested specific pressure distribution and mass flow rate measurements in microchannels of various cross sections. Kuddusi et al. [14] studied the thermal and hydrodynamic characters of a hydrodynamically developed and thermally developing flow in trapezoidal silicon microchannels. It was found that the friction factor decreases if rarefaction and/or aspect ratio increase. Their work also showed that at low rarefactions the very high heat transfer rate at the entrance diminishes rapidly as the thermally developing flow approaches fully developed flow. Chen et al. [15] investigated the mixing characteristics of flow through microchannels with wavy surfaces. However, they modeled the wavy surface as a series of rectangular steps which seems to cause computational errors at boundary especially in micro-scale geometry. Also their working fluid was liquid and they imposed no-slip boundary conditions at the microchannel wall surface. Recently, Shokouhmand and Bigham [16] investigated the developing fluid flow and heat transfer through a wavy microchannel with numerical methods in curvilinear coordinate. They took the effects of creep flow and viscous dissipation into account. Their results showed that Knudsen number has declining effect on both the $C_f.Re$ and Nusselt number on the undeveloped fluid flow. Furthermore, it was observed that the effect of viscous dissipation has a considerable effect in microchannels. This effect can be more significant by increasing Knudsen number. Also, it leads a singular point in Nusselt profiles. In addition, in two another articles, Shokouhmand et al. [17] and Bigham et al. [18] probed the developing fluid flow and heat transfer through a constricted microchannel with numerical methods in curvilinear coordinate. In these two works, several effects had been considered.

The main purpose of this chapter is to explain the details of finding the fluid flow and heat transfer patterns with numerical methods in slip flow regime through curvilinear microchannels. Governing equations including continuity, momentum and energy with the velocity slip and temperature jump conditions at the solid walls are discretized using the finite-volume method and solved by SIMPLE algorithm in curvilinear coordinate. In addition, this chapter explains how the effects of creep flow and viscous dissipation can be assumed in numerical methods in curvilinear microchannels.

2. Physical model and governing equations

To begin with, Fig. 1 shows the geometry of interest which is seen to be a two-dimensional symmetric constricted microchannel. The channel walls are assumed to extend to infinity in the z-direction (i.e., perpendicular to the plane). Steady laminar flow with constant properties is considered. The present work is concerned with both thermally and hydrodynamically developing flow cases. In this study the usual continuum approach is coupled with two main characteristics of the micro-scale phenomena, the velocity slip and the temperature jump. A general non-orthogonal curvilinear coordinate framework with (ξ,η) as independent variables is used to formulate the problem.

The mathematical non-dimensional expression of constricted wall is given as

$$y_w(x) = -0.5 + a(1 - \cos(2\pi(\frac{x}{\lambda} - 0.125)))$$ (1)
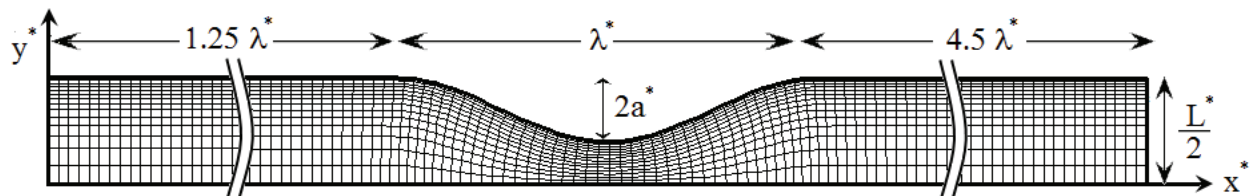
Fig. 1. Physical domain of constricted microchannel

Here, the governing equations in their basic forms are introduced:
Continuity equation:
For an arbitrary control volume *CV* fixed in space and time, conservation of mass requires that the rate of change of mass within the control volume is equal to the mass flux crossing the control surface *CS* of *CV*, i.e.

$$\frac{\partial}{\partial t} \int_{CV} \rho^* d^* \forall^* + \int_{CS} \rho^* \vec{u}^* . d^* \vec{A}^* = 0 \tag{2}$$

Using the Gauss (divergence) theorem, the surface integral may be replaced by a volume integral. Then becomes

$$\int_{CV} \left[\frac{\partial \rho^*}{\partial t} + \nabla^* . (\rho^* \vec{u}^*) \right] d^* \forall^* = 0 \tag{3}$$

Since is valid for any size of *CV*, it implies that

$$\frac{\partial \rho^*}{\partial t} + \nabla^* . (\rho^* \vec{u}^*) = 0 \tag{4}$$

For incompressible flow, in 2D Cartesian coordinates becomes

$$\frac{\partial (u^*)}{\partial x^*} + \frac{\partial (v^*)}{\partial y^*} = 0 \tag{5}$$

Momentum equations:
Newton's second law of motion states that the time rate of changes of linear momentum is equal to the sum of the forces acting. For a control volume *CV* fixed in space and time with flow allowed to occur across the boundaries, the following equation is available:

$$\frac{\partial}{\partial t} \int_{CV} \rho^* \vec{u}^* d^* \forall^* + \int_{CS} \rho^* u^* \vec{u}^* d^* \vec{A}^* = \sum \vec{F}^* \tag{6}$$

By the Gauss theorem and continuity equation, becomes:

$$\rho^* \frac{D^* \vec{U}}{D^* t} = \rho^* \vec{f}^* - \nabla^* p^* + \nabla^* . \tau^*_{i.j} \tag{7}$$

Substitution of viscous stress tensor into above equation gives the Navier-Stokes equations

$$\frac{\partial}{\partial x^*}(\rho^* u^{*2}) + \frac{\partial}{\partial y^*}(\rho^* u^* v^*) = -\frac{\partial p^*}{\partial x^*} + \mu(\frac{\partial^2 u^*}{\partial x^{*2}} + \frac{\partial^2 u^*}{\partial y^{*2}}) + \rho^* g_x \tag{8}$$

$$\frac{\partial}{\partial x^*}(\rho^* u^* v^*) + \frac{\partial}{\partial y^*}(\rho^* v^{*2}) = -\frac{\partial p^*}{\partial y^*} + \mu(\frac{\partial^2 v^*}{\partial x^{*2}} + \frac{\partial^2 v^*}{\partial y^{*2}}) + \rho^* g_y \tag{9}$$

Energy equation:
The first law of thermodynamics states that the time rate of change of internal energy plus kinetic energy is equal to the rate of heat transfer less the rate of work done by the system. For a control volume *CV* this can be written as

$$\frac{\partial}{\partial t}\int_{CV} \rho^* e^* d\forall^* + \int_{CS} \rho^* e^* \vec{u}^* d\vec{A}^* = \frac{dE}{dt} = \dot{Q} - \dot{W} \tag{10}$$

Applying the Gauss theorem and shrinking the volume to zero and then substituting the Fourier law of heat conduction gives

$$\frac{\partial(\rho^* C_P u^* T)}{\partial x^*} + \frac{\partial(\rho^* C_P v^* T)}{\partial y^*} = \frac{\partial}{\partial x^*}\left(k\frac{\partial T}{\partial x^*}\right) + \frac{\partial}{\partial y^*}\left(k\frac{\partial T}{\partial y^*}\right) + \Phi^* \tag{11}$$

$$\Phi^* = \mu[2\left(\frac{\partial u^*}{\partial x^*}\right)^2 + 2\left(\frac{\partial v^*}{\partial y^*}\right)^2 + \left(\frac{\partial u^*}{\partial y^*} + \frac{\partial v^*}{\partial x^*}\right)^2]$$

where Φ represents the dissipation function stems from viscous stresses.
Non-dimensional variables are introduced as

$$x = \frac{x^*}{L^*}, y = \frac{y^*}{L^*}, u = \frac{u^*}{u_i^*}, v = \frac{v^*}{u_i^*}, p = \frac{p^*}{\rho_i^* u_i^{*2}}, \theta = \frac{T - T_i}{T_w - T_i}$$

$$\mathrm{Re}_i = \frac{\rho_i^* u_i^* L^*}{\mu}, Pe_i = \mathrm{Re}_i \mathrm{Pr}_i = \frac{u_i^* L^*}{\alpha}, Ec_i = \frac{u_i^{*2}}{C_p(T_w - T_i)}$$

Here, Ec_i means the Eckert number.
Then, non-dimensional governing equations are obtained as
Non-dimensional continuity equation:

$$\frac{\partial(u)}{\partial x} + \frac{\partial(v)}{\partial y} = 0 \tag{12}$$

Non-dimensional momentum equations:

$$\frac{\partial}{\partial x}(u^2) + \frac{\partial}{\partial y}(uv) = -\frac{\partial p}{\partial x} + \frac{1}{\mathrm{Re}_i}(\frac{\partial^2 u}{\partial x^2} + \frac{\partial^2 u}{\partial y^2}) \tag{13}$$

$$\frac{\partial}{\partial x}(uv) + \frac{\partial}{\partial y}(v^2) = -\frac{\partial p}{\partial y} + \frac{1}{\mathrm{Re}_i}(\frac{\partial^2 v}{\partial x^2} + \frac{\partial^2 v}{\partial y^2}) \tag{14}$$

Non-dimensional energy equation:

$$\frac{\partial(u\theta)}{\partial x} + \frac{\partial(v\theta)}{\partial y} = \frac{1}{Pe_i}\left(\frac{\partial^2\theta}{\partial x^2} + \frac{\partial^2\theta}{\partial y^2}\right) + \Phi$$

(15)

$$\Phi = \frac{Ec_i}{Re_i}[2\left(\frac{\partial u}{\partial x}\right)^2 + 2\left(\frac{\partial v}{\partial y}\right)^2 + \left(\frac{\partial u}{\partial y} + \frac{\partial v}{\partial x}\right)^2]$$

3. Grid generation

Grid generation technique can be classified into three groups
1. Algebraic Methods.
2. Conformal mappings based on complex variables.
3. Partial differential methods.
Algebraic and differential techniques can be used to complicate three dimensional problems, but for the method available for generating grids these two schemes show the most promise for continued development and can be used in conjunction with finite difference methods.
Because the governing equations in fluid dynamics contain partial differentials and are too difficult in most cases to solve analytically, these partial differential equations are generally replaced by the finite volume terms. This procedure discretizes the field into a finite number of states, in order to get the solution.
The generation of a grid, with uniform spacing, is a simple exercise within a rectangular physical domain. Grid points may be specified as coincident with the boundaries of the physical domain, thus making specification of boundary conditions considerably less complex. Unfortunately, the physical domain of interest is nonrectangular. Therefore, imposing a rectangular computational domain on this physical domain requires some interpolation for the implementation of the boundary conditions. Since the boundary conditions have a dominant influence on the solution such an interpolation causes inaccuracy at the place of greatest sensitivity. To overcome these difficulties, a transformation from physical space to computational space is introduced. This transformation is accomplished by specifying a generalized coordinate system, which will map the nonrectangular grid system, and change the physical space to a rectangular uniform grid spacing in the computational space.
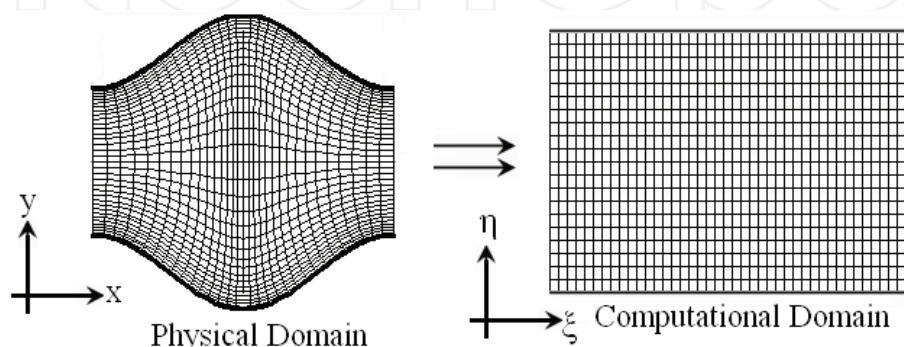

Fig. 2. Physical and computational domains

Transformation between physical (x,y) and computational (ξ,η) domains, important for body-fitted grids. Define the following relations between the physical and computational spaces:

$$\begin{aligned} \xi &= \xi(x,y) \\ \eta &= \eta(x,y) \end{aligned}$$

(16)

The chain rule for partial differentiation yields the following expression:

$$\begin{aligned} \frac{\partial}{\partial x} &= \xi_x \frac{\partial}{\partial \xi} + \eta_x \frac{\partial}{\partial \eta} \\ \frac{\partial}{\partial y} &= \xi_y \frac{\partial}{\partial \xi} + \eta_y \frac{\partial}{\partial \eta} \end{aligned}$$

(17)

From above equations the following differential expressions are obtained

$$\begin{aligned} d\xi &= \xi_x dx + \xi_y dy \\ d\eta &= \eta_x dx + \eta_y dy \end{aligned}$$

(18)

which are written in a compact form as

$$\begin{bmatrix} d\xi \\ d\eta \end{bmatrix} = \begin{bmatrix} \xi_x & \xi_y \\ \eta_x & \eta_y \end{bmatrix} \begin{bmatrix} dx \\ dy \end{bmatrix}$$

(19)

Reversing the role of independent variables, i.e.,

$$\begin{aligned} x &= x(\xi,\eta) \\ y &= y(\xi,\eta) \end{aligned}$$

(20)

The following may be written

$$\begin{aligned} dx &= x_\xi d\xi + x_\eta d\eta \\ dy &= y_\xi d\xi + y_\eta d\eta \end{aligned}$$

(21)

In a compact form they are written as

$$\begin{bmatrix} dx \\ dy \end{bmatrix} = \begin{bmatrix} x_\xi & x_\eta \\ y_\xi & y_\eta \end{bmatrix} \begin{bmatrix} d\xi \\ d\eta \end{bmatrix}$$

(22)

Comparing equations 19 and 22, it can be concluded that

$$\begin{bmatrix} \xi_x & \xi_y \\ \eta_x & \eta_y \end{bmatrix} = \begin{bmatrix} x_\xi & x_\eta \\ y_\xi & y_\eta \end{bmatrix}^{-1}$$

(23)

From which

$$x_\xi = +J\eta_y \; , \; x_\eta = -J\xi_y \; , \; y_\xi = -J\eta_x \; , \; y_\eta = -J\xi_x$$

(23)

Where

$$J = x_\xi y_\eta - x_\eta y_\xi \qquad (23)$$

and is defined as the Jacobian of transformation [19].

4. Governing equations in computational space

To formulate the problem, a continuum based approach is used. Here (ξ, η) are independent variables in general non-orthogonal curvilinear coordinate. The nondimensional governing equations can be written as:

Non-dimensional continuity equation in curvilinear coordinate:

$$\frac{\partial U^C}{\partial \xi} + \frac{\partial V^C}{\partial \eta} = 0 \qquad (24)$$

Non-dimensional momentum equations in curvilinear coordinate:

$$\frac{\partial}{\partial \xi}(uU^C) + \frac{\partial}{\partial \eta}(uV^C) = \frac{1}{Re_i}\{\frac{\partial}{\partial \xi}(q_{11}\frac{\partial u}{\partial \xi}) + \frac{\partial}{\partial \eta}(q_{22}\frac{\partial u}{\partial \eta}) + \frac{\partial}{\partial \xi}(q_{12}\frac{\partial u}{\partial \eta}) + \frac{\partial}{\partial \eta}(q_{12}\frac{\partial u}{\partial \xi})\}$$
$$-\frac{\partial}{\partial \xi}(y_\eta p) + \frac{\partial}{\partial \eta}(y_\xi p) \qquad (25)$$

$$\frac{\partial}{\partial \xi}(vU^C) + \frac{\partial}{\partial \eta}(vV^C) = \frac{1}{Re_i}\{\frac{\partial}{\partial \xi}(q_{11}\frac{\partial v}{\partial \xi}) + \frac{\partial}{\partial \eta}(q_{22}\frac{\partial v}{\partial \eta}) + \frac{\partial}{\partial \xi}(q_{12}\frac{\partial v}{\partial \eta}) + \frac{\partial}{\partial \eta}(q_{12}\frac{\partial v}{\partial \xi})\}$$
$$+\frac{\partial}{\partial \xi}(x_\eta p) - \frac{\partial}{\partial \eta}(x_\xi p) \qquad (25)$$

Non-dimensional energy equation in curvilinear coordinate:

$$\frac{\partial}{\partial \xi}(\theta U^C) + \frac{\partial}{\partial \eta}(\theta V^C) = \frac{1}{Pe_i}\{\frac{\partial}{\partial \xi}(q_{11}\frac{\partial \theta}{\partial \xi}) + \frac{\partial}{\partial \eta}(q_{22}\frac{\partial \theta}{\partial \eta}) + \frac{\partial}{\partial \xi}(q_{12}\frac{\partial \theta}{\partial \eta}) + \frac{\partial}{\partial \eta}(q_{12}\frac{\partial \theta}{\partial \xi})\} + \Phi \quad (26)$$

$$\Phi = \frac{Ec_i}{Re_i J}\{2(u_\xi y_\eta - u_\eta y_\xi)^2 + 2(-v_\xi x_\eta + v_\eta x_\xi)^2 + (-u_\xi x_\eta + u_\eta x_\xi + v_\xi y_\eta - v_\eta y_\xi)^2\}$$

Where

$$U^C = uy_\eta - vx_\eta \, , V^C = -uy_\xi + vx_\xi \, , J = x_\xi y_\eta - x_\eta y_\xi$$

$$q_{11} = \frac{1}{J}(y_\eta^2 + x_\eta^2) \, , q_{12} = \frac{-1}{J}(x_\xi x_\eta + y_\xi y_\eta) \, , q_{22} = \frac{1}{J}(x_\xi^2 + y_\xi^2)$$

where Φ is viscous dissipation function that shows the effects of viscous stresses. u and v are the velocity components and U^C and V^C are the velocities in ξ, η.

5. Surface effects and boundary conditions

As gas flows through conduits with micron scale dimensions or in low pressures conditions, a sublayer called Knudsen layer starts growing. Knudsen layer begins to become dominant between the bulk of the fluid and wall surface. This sublayer is on the order one mean free path and for Kn≤0.1 is small in comparison with the microchannel height. So it can be ignored by extrapolating the bulk gas flow towards the walls. This causes a finite velocity slip value at the wall, and a nonzero difference between temperature of solid boundaries and the adjacent fluid. It means a slip flow and a temperature jump will be present at solid boundaries. This flow regime is known as the slip flow regime. In this flow regime, the Navier–Stokes equations are still valid together with the modified boundary conditions at the wall [20-23].

To calculate the slip velocity at wall under rarified condition, the Maxwell slip condition has been widely used which is based on the first-order approximation of wall-gas interaction from kinetic theory of gases. Maxwell supposed on a control surface, s, at a distance δ/2, half of the molecules passing through s are reflected from the wall, the other half of the molecules come from one mean free path away from the surface with tangential velocity u_λ. It was supposed that a fraction σ_v of the molecules are reflected diffusively at the walls and the remaining (1-σ_v) of the molecules are reflected specularly, Maxwell obtained the following expression by using Taylor expansion for u_λ about the tangential slip velocity of the gas on this surface namely us. In this work, by using von-Smoluchowski model we have the following boundary conditions at wall in curvilinear coordinate form [20-23]:

$$U_s = \frac{2-\sigma_v}{\sigma_v} Kn_i \left.\frac{\partial U_s}{\partial n}\right|_w + \frac{3}{2\pi}\frac{(1-\gamma)}{\gamma}\left(\frac{Kn^2 \mathrm{Re}}{Ec}\right)_i \left.\frac{\partial \theta}{\partial s}\right|_w \tag{27}$$

$$\theta_s = 1 - \left(\frac{2-\sigma_T}{\sigma_T}\right)\left(\frac{2\gamma}{\gamma+1}\right)\left(\frac{Kn}{\mathrm{Pr}}\right)_i \left.\frac{\partial \theta}{\partial n}\right|_w \tag{28}$$

where, Pr and Kn mean the Prandtl number and Knudsen number, respectively. The Knudsen number shows the effect of rarefaction on flow properties. Also γ and σ represent the specific heat ratio and accommodation coefficient, respectively. For slip velocity, the effect of thermal creep is taken into account. The thermal creep which is a rarefaction effect shows that even without any pressure gradient the flow can be caused due to tangential temperature gradient, specifically from colder region toward warmer region. This effect also can be important in causing variation of pressure along microchannels in the presence of tangential temperature gradients. In addition, the other boundary conditions used are as follows. A uniform inlet velocity and temperature are specified as

$$u = 1, v = 0, \theta = 0 \tag{29}$$

In the outlet, fully developed boundary conditions are assumed as

$$\frac{\partial u}{\partial x} = \frac{\partial v}{\partial x} = \frac{\partial \theta}{\partial x} = 0 \tag{30}$$

Also in this work, C_f. Re and Nusselt number are obtained using the following equations.

$$C_f \, \mathrm{Re} = \frac{4 \, (y_w(x))^2}{\left(\int u(x,y) \, dy\right)^2} \frac{\partial u^{tang}(x)}{\partial n} \tag{31}$$

$$Nu = \frac{1}{\theta_{ave}(x) - 1} \frac{\partial \theta(x)}{\partial n}\bigg|_w \tag{32}$$

where $y_w(x)$ represents the half width of microchannel and θ_{ave} is the nondimensional average temperature of fluid.

6. Numerical solution

In the present work, the slip flow regime with the Knudsen number ranging from 0.01 to 0.1 is considered. The study is limited to incompressible flow. Flow with Mach number lower than 0.3 can be assumed incompressible. The following equation is used to check this limit [22].

$$\mathrm{Re} = \frac{Ma}{Kn} \sqrt{\frac{\pi \gamma}{2}} \tag{33}$$

SIMPLE algorithm in non-orthogonal curvilinear coordinate framework is used to solve the governing equations with appropriate boundary conditions [24]. A fully implicit scheme is used for the temporal terms and the HYBRID differencing [25] is applied for the approximation of the convective terms. A full-staggered grid is applied in which scalar variables such as pressure and temperature at ordinary points are evaluated but velocity components are calculated around the cell faces. Also the control volumes for u and v are different from the scalar control volumes and different from each other. The Poisson equations is solved for (x, y) to find grid points [19] and are distributed in a nonuniform manner with higher concentration of grids close to the curvy walls and normal to all walls, as shown in Fig. 1. In this work, two convergence criteria have been imposed. First convergence criterion is a mass flux residual less than 10^{-8} for each control volume. Another criteria that is established for the steady state flow is $(|\varphi_{i+1} - \varphi_i|)/|\varphi_{i+1}| \leq 10^{-10}$ where φ represents any dependent variable, namely u, v and θ, and i is the number of iteration.

The numerical code and non-orthogonal grid discretization scheme used in the present study have been validated in Fig. 3.a. against the previously published results of Wang and Chen [11]. Their model is similar to the present model, but water was used as a working fluid and the channel scale was macro. The slip effects approximately exterminated with fixing Kn number at zero.

To investigate the accuracy of the used numerical model for the special case of microchannel, the obtained numerical results for slip flow are compared with analytical results of microchannel in [26]. The used parameters in [26] for nondimensional temperature and Nusselt number can be shown in terms of this work as follows:

$$\theta = 1 + 6Ec_i \mathrm{Pr}(1 - \frac{u_s}{u_m})[3(1-y)^2 y^2 + \frac{u_s}{u_m}\{(y-y^2)[1-3(y-y^2)] + 2\beta_T Kn\}] \tag{34}$$

$$Nu_\infty = 420\frac{u_s}{u_m}[27 + (9 + 420\beta_t Kn)\frac{u_s}{u_m} - (\frac{u_s}{u_m})^2]^{-1} \tag{35}$$

Which

$$\beta_v = \frac{2 - \sigma_v}{\sigma_v} , \beta_T = \frac{2 - \sigma_T}{\sigma_T}\frac{2\gamma}{1 + \gamma}\frac{1}{Pr} \tag{23}$$
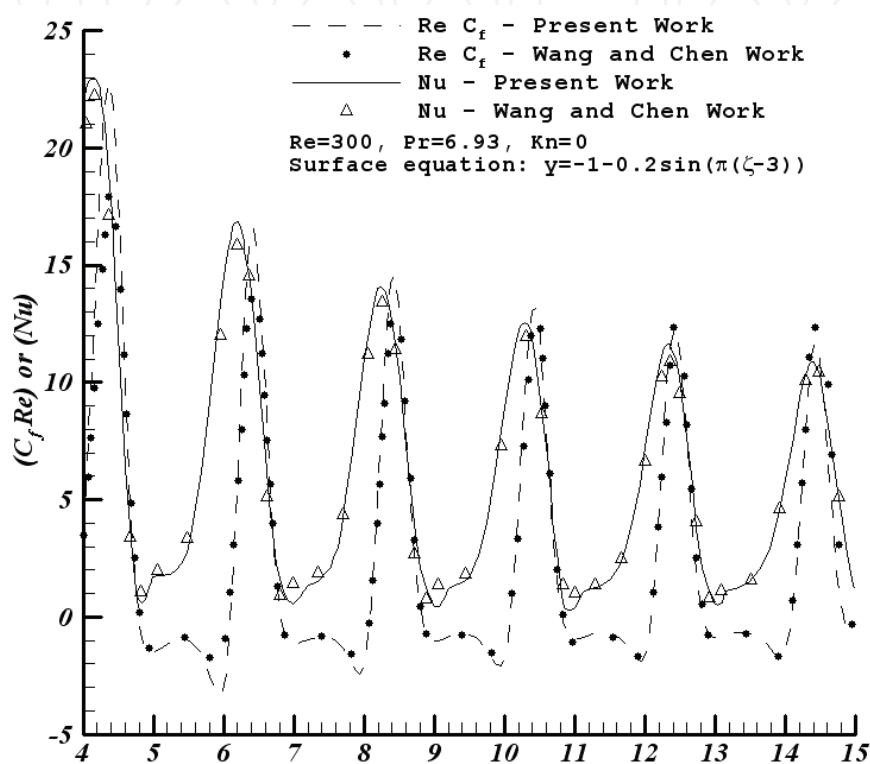

Fig. 3a. Validation of the numerical code with available data

This comparison is carried out for the Kn=0.04, Pr=0.7, Pe=0.5, Ec=0.286, β_v =1 and β_T=1.667. In the numerical code, two dimensional forms are considered for the convective and diffusive terms. To compare the analytical and numerical solutions, the viscous dissipation term in the analytical solution is also added to the numerical solution. Also the flow work term in the analytical solution is considered in the numerical model. The analytical solution results 3.47 for the Nusselt number, while the numerical model gives 3.53 for the fully developed Nusselt number which are in a good agreement. Furthermore, the nondimensional temperature profiles for the two models are shown in Fig. 3.b. which are also in a good agreement.

To ensure that the results of the numerical study are independent of the computational grid; a grid sensitivity analysis is performed for steady state. In this work, three meshes are used in numerical simulation: 350×65, 400×75 and 450×85. Generally, the accuracy of the solution and the time required for the solution are dependent on mesh refinement. In this work, the optimum grid is searched to have appropriate run-time and enough accuracy. As it is shown in Fig. 4, the obtained solution with mentioned grids shows sufficient accuracy. For Kn=0.075 at Re=2, 400×75 grid seems to be optimum in accuracy and run-time. Grid

dependence studies have been completed with similar results for each numerical solution presented in the results section. However, throughout this study the results are only presented for the optimum grid.
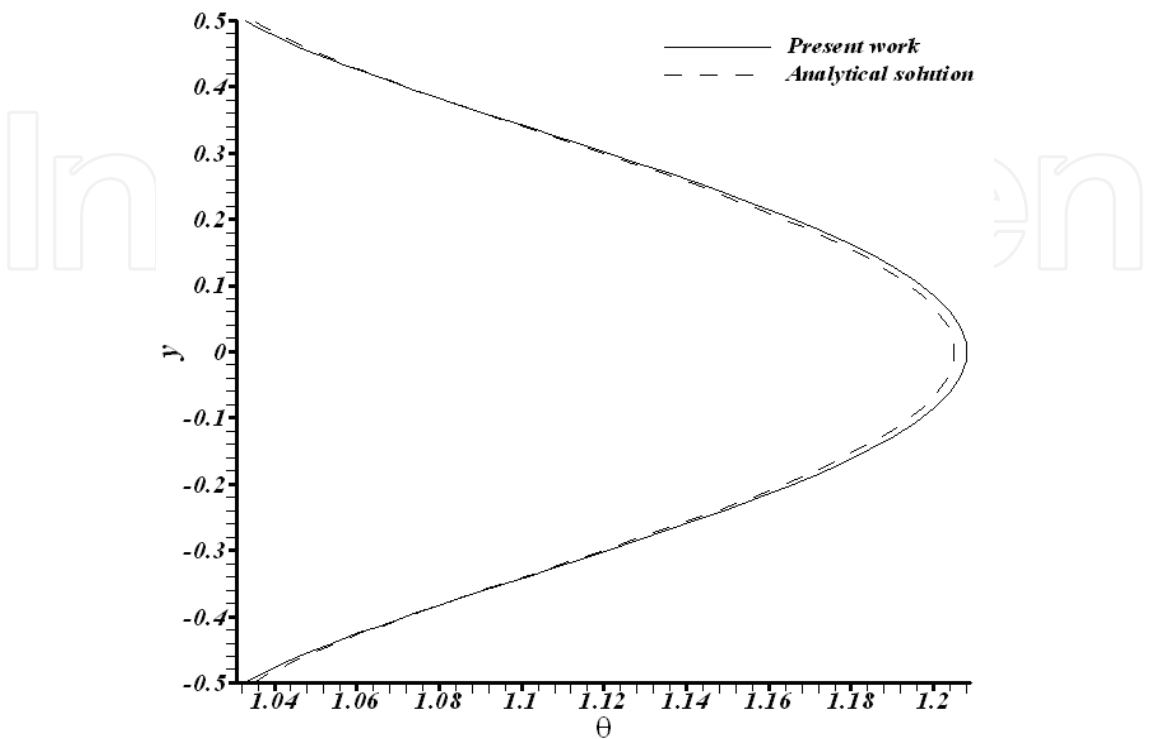

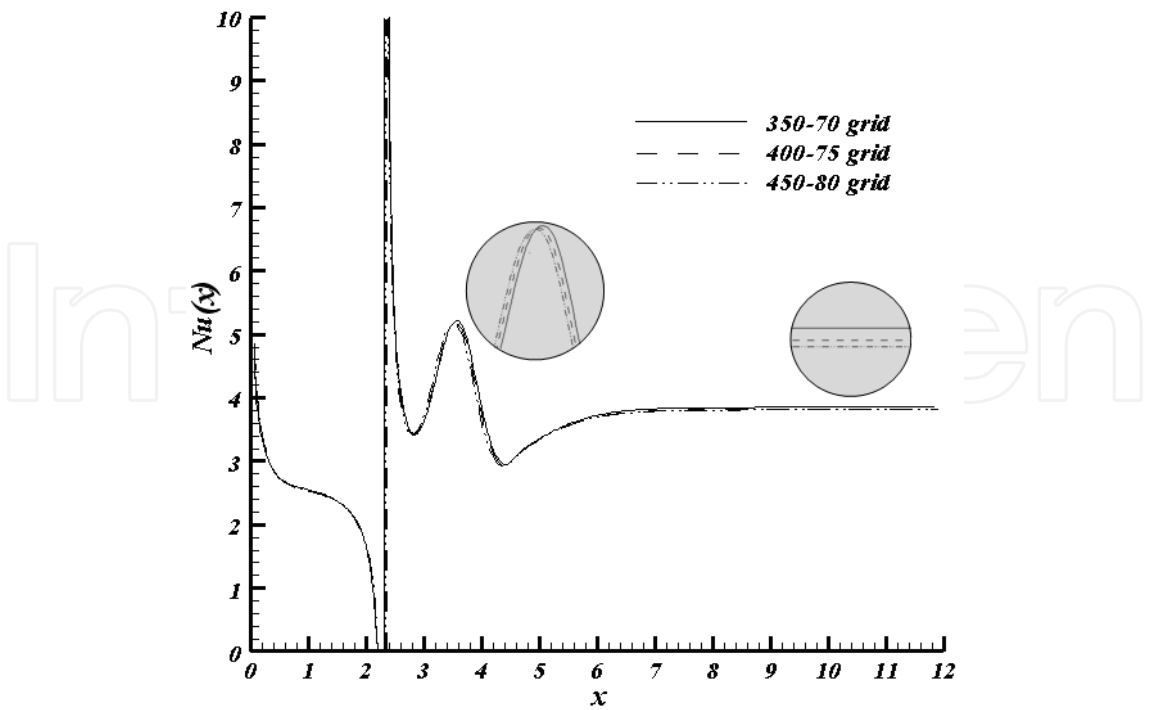Fig. 3b. Validation of the numerical code with available data

Fig. 4. Numerical results of local Nusselt number along the constricted microchannel with KN=0.075 at Re=2 and a=0.15

7. Results and discussion

To have a clear understanding of the problem and studding the fluid flow and heat transfer characteristics (e.g. the velocity field, local temperature field, friction factor and local Nusselt number), numerical simulation is performed for different values of Knudsen numbers and various amplitude values. Because of the symmetrical geometry, in this work, only one half of microchannel shown in Fig. 1 is numerically solved. Therefore, the run-time reduces considerably. However, the results depicted for the whole microchannel. The results are obtained for γ=1.4, Pr=0.7, σ_T=0.9 and σ_v=0.9. Also surface wavelength is taken λ=2. The boundaries are maintained at temperature T_w=70 °C and the uniform inlet temperature is considered T_i=25 °C. Furthermore, the five studied Knudsen numbers and corresponding Eckert number is shown in Table 1.

	Kn=0.01	Kn=0.025	Kn=0.05	Kn=0.075	Kn=0.1
Ec	4.82×10^{-4}	3.01×10^{-3}	1.21×10^{-2}	2.71×10^{-2}	4.82×10^{-2}

Table 1. Numerical values for Ec as a function of Kn at Re=2

7.1 The flow field

The effect of Kn on slip velocity for hydrodynamically/thermally developing flow in the constricted microchannel is depicted in Fig. 5. As observed the slip velocity experiences a rapid jump in the convergent region at each Knudsen number. In the convergent region, the cross section area decreases and causes the acceleration of the fluid flow. So the average velocity increases and this increase contributes to a rapid raise in the slip velocity in this region. In addition, as the rarefaction effect increases, the slip velocity increases. By increasing the Knudsen number, the channel dimensions decrease and approach to molecular dimensions. Physically, decreasing channel dimensions causes a decline in the interaction of gaseous molecules with the adjacent walls. So the momentum exchange between the fluid and adjacent walls declines. In other words, the fluid molecules are lesser affected by the walls that leads to larger slip velocity. The increase in slip velocity can be explained in other words. As the microchannel dimensions decrease, the MFP (mean free path) becomes more comparable with the microchannel's characteristic length in size. This means that the thickness of Knudsen layer increases that causes an increase in the slip velocity.

A schematic comparison between the velocity profile in different Knudsen numbers and in different cross sections is carried out in Fig. 6. As expected, as the fluid approaches the throttle region, the slip velocity gets higher value. As expected also, by intensification of rarefaction effect, the slip velocity increases.

Fig. 7 displays $C_f.Re$ versus Knudsen number for hydrodynamically/thermally developing flow in the constricted microchannel. As shown, due to presence of high velocity gradients, there is high friction in the entrance of channel. As expected, as flow develops, this high friction rapidly declines. Furthermore, when fluid flows in the convergent region, $C_f.Re$ experiences a rapid decrease in the microchannel. By referring to the definition of $C_f.Re$ in Eq. (31), it can be noticed that there are three parameters affecting the behavior of $C_f.Re$. The first parameter is the square of channel width that decreases through the convergent region. The second parameter is the inverse of square of the average velocity that decreases in the convergent region. And finally the third parameter is the gradient of tangential velocity, $\partial u^{tang}(x)/\partial n$ that increases in this region because of increase of the average velocity through this area. Here, it seems that the effects of the first and second parameter are dominant and make the $C_f.Re$ reduce in the convergent part. Furthermore, rarefaction has a decreasing effect

on the friction factor. As rarefaction increases, the slip velocity increases which results in a flatter velocity profile and consequently reduces the wall velocity gradient. This reduction contributes to the decrease of $C_f.Re$ with Knudsen number. For instance, by variation of Knudsen number from 0.01 to 0.1, the $C_f.Re$ at the end of microchannel decreases 38%. Moreover, physically by increasing the Knudsen number, the interaction of gaseous molecules with the adjacent walls decreases. Therefore, the momentum exchange between the fluid and adjacent walls reduces and this means $C_f.Re$ declines.
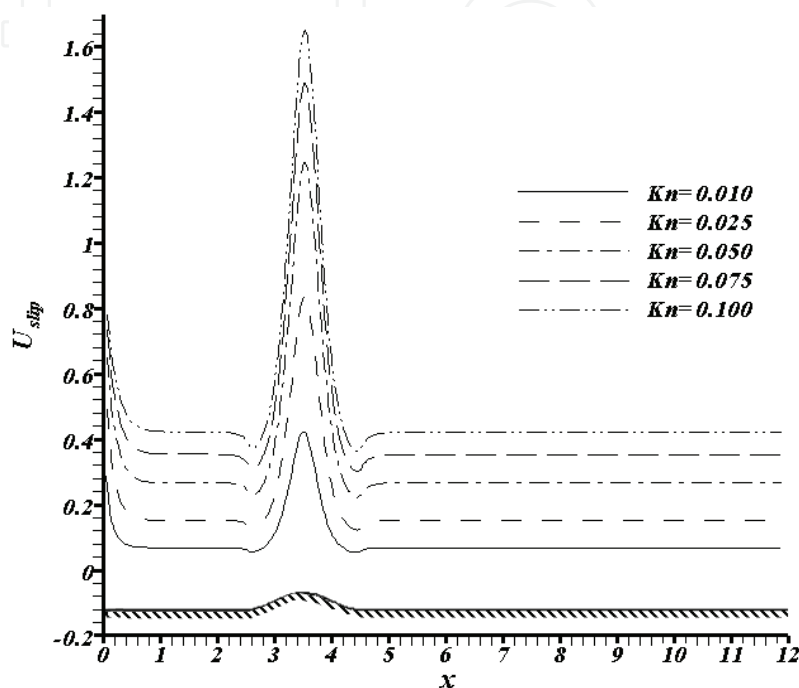
Fig. 5. Variation of slip velocity along the constricted microchannel with Knudsen number Re=2 and a=0.15
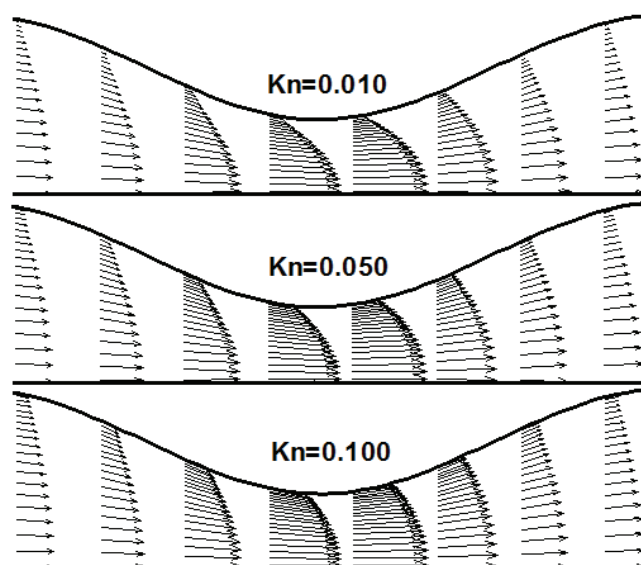
Fig. 6. Schematic illustration of Knudsen number effect on velocity profile at Re=2 and a=0.15
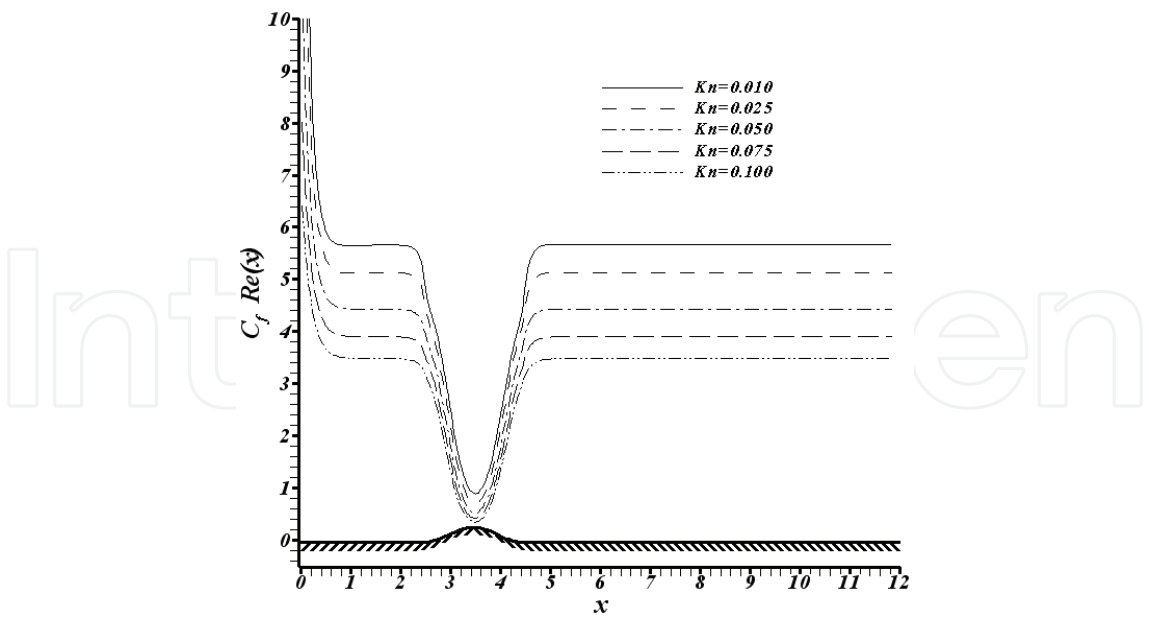
Fig. 7. Variation of $C_f.Re$ along the constricted microchannel with Knudsen number at Re=2 and a=0.15

In Fig. 8 the variation of $C_f.Re$ as a function of the amplitude of wave is shown, while keeping the Reynolds number and Knudsen number constant. As shown, by decreasing the amplitude of the wave (i.e., increasing the constriction), the fluid flow senses the variation of cross section more. In other words, by decreasing the amplitude of the wave and consequently the more increase in the average velocity, $C_f.Re$ experiences more intense decrease in the convergent region. For instance, by variation of amplitude of the wave from 0.05 to 0.15, the $C_f.Re$ decreases 82% in the throttle region.
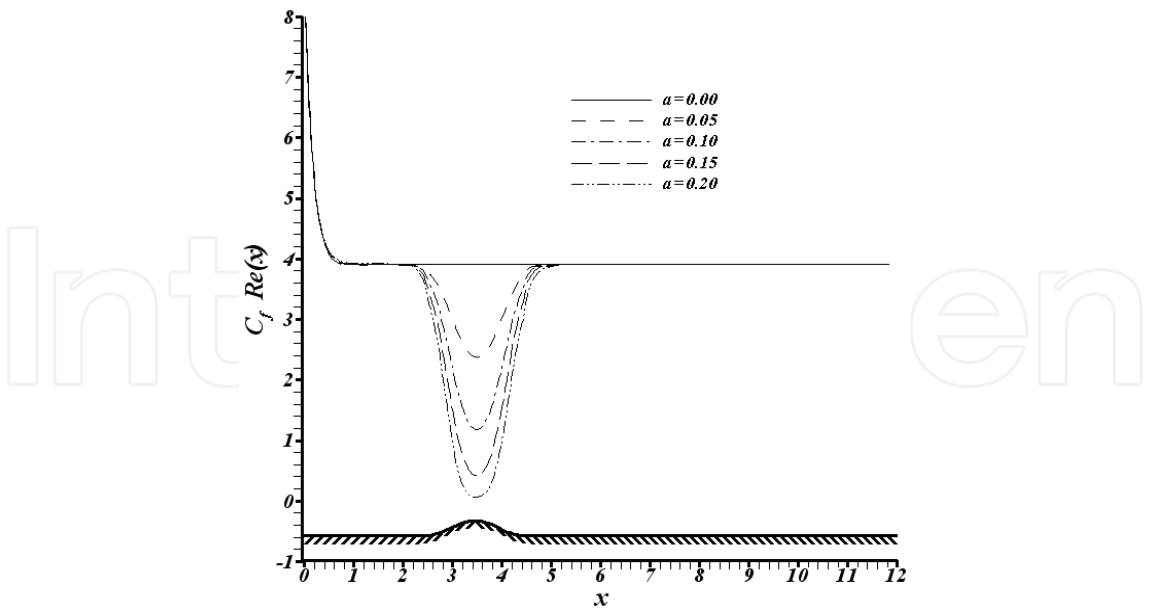
Fig. 8. Variation of $C_f.Re$ along the constricted microchannel with amplitude of the wave at Re=2 and Kn=0.075

A comparison is carried out in Fig. 9 to investigate the effect of viscous dissipation on $C_f.Re$. As shown, viscous dissipation inconsiderably affects $C_f.Re$.
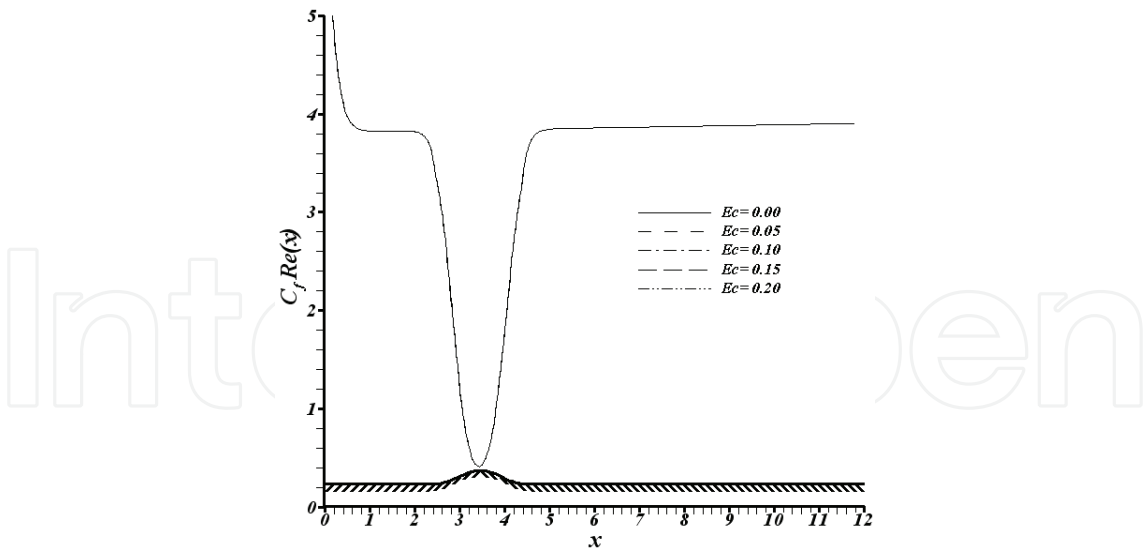
Fig. 9. Variation of local $C_f.Re$ with Eckert number at Re=2, Kn=0.075 and a=0.15

7.2 The temperature field

To clearly understand the physic of fluid flow, the isothermal lines corresponds to the non-dimensional temperature of unity for five studies Knudsen number are illustrated in Fig. 10. As observed, these isothermal lines clearly divide the physical domain in to two different regions, the region of $\theta<1$ in the inlet of channel and the region of $\theta>1$ in the outlet of channel. In the region of $\theta<1$, where the non-dimensional temperature is less than unity, the fluid receives energy from the adjacent walls, as the fluid flows through the channel. This energy transfer from the walls to the fluid continues till the fluid approaches the region close to $\theta=1$ where the heat supplied by the walls is balanced by the internal heat generation due to viscous heating. After this region, the internal heat generated by viscous dissipation gets to such a high value that completely reverse the direction of heat transfer. In other words, in the region of $\theta>1$, the net energy exchange is from the fluid towards the walls. With the above descriptions, it can be found that viscous dissipation plays an important role in this kind of flows. Furthermore, the effect of viscous dissipation on fluid flow is more considerable in higher Knudsen number as the region of $\theta>1$ expands.
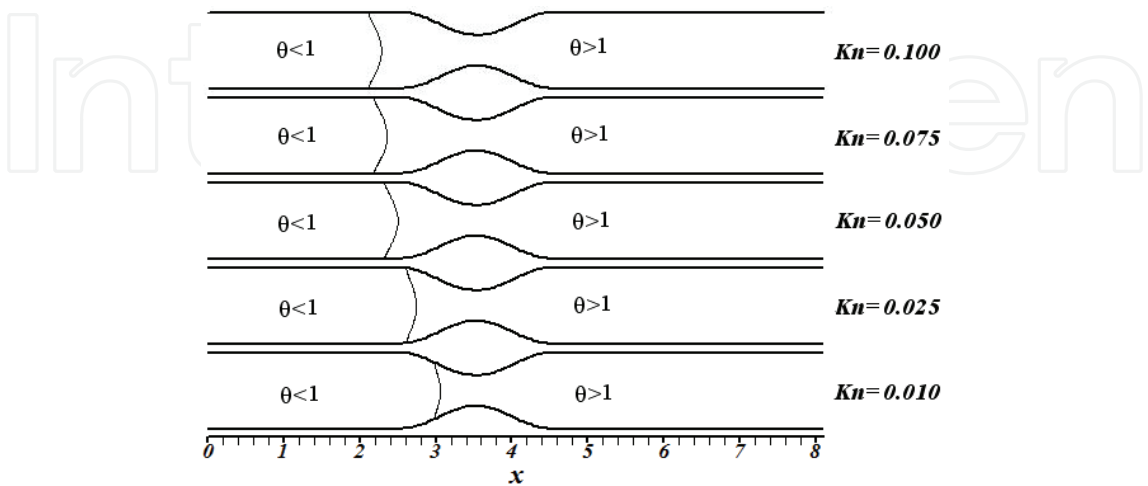

Fig. 10. Isothermal line corresponds to non-dimensional temperature unity along the constricted microchannel with Knudsen number at Re=2 and a=0.15

Fig. 11 shows the effect of Knudsen number on temperature jump. By increasing the Knudsen number and consequently the decreasing of channel dimensions, the thickness of Knudsen layer increases. This increase leads to greater temperature jumps. However it should be noted that this increase in temperature jump shows itself in two different ways. In the inlet of microchannel, the fluid temperature near the wall is less than wall temperature and this increase can be seen by lesser fluid temperature near the wall. While in the outlet of channel, as the fluid temperature is higher than wall temperature, this increase can be noticed by higher fluid temperature near the wall. For instance, in the outlet of channel for Kn=0.1, the nondimensional fluid temperature near the wall is more than 1.01. Furthermore, it can be noticed that the fluid temperature near the wall generally increases along the microchannel. However, due to the convergent region, the fluid temperature at each Knudsen number experiences a jump in this region. Moreover, in the developed region, the fluid temperature near the wall approaches to a constant value.
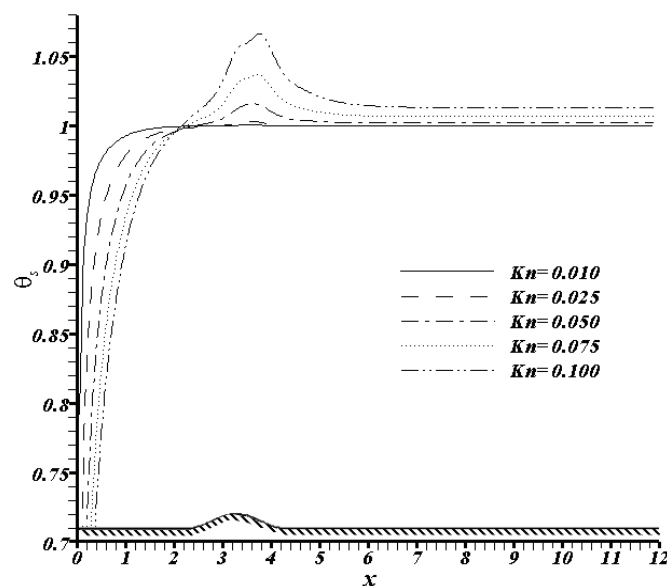
Fig. 11. Variation of the fluid temperature near the wall with Knudsen number along the constricted microchannel at Re=2 and a=0.15

The variation of average temperature along the microchannel versus Knudsen number is illustrated in Fig. 12. As shown, in the entrance region of microchannel, the Knudsen number has a decreasing effect on the average temperature. In this region, as the Knudsen number increases, the fluid enters with greater inlet velocity and momentum and consequently exchange less energy with the adjacent walls. Therefore, the average temperature decreases. To study the effect of Knudsen number in the outlet region, one should consider the effect of viscous dissipation due to importance of this effect is in this region. By increasing the rarefaction effect, the velocity gradients become more considerable and consequently the effect of viscous dissipation increases. Viscous dissipation acts like a thermal source that tends to increase the average fluid temperature. In addition, due to the convergent region, the average fluid temperature at each Knudsen number experiences a jump in this region.

In Fig. 13 and Fig. 14, temperature distribution in two different cross sections at x= 0.75λ, 2.5λ are presented. The temperature distribution in Fig. 13 is located in the region corresponds to $\theta<1$(the inlet region with lower viscous dissipation effects). In this region, as expected with larger Knudsen number, we have higher temperature jump at the wall and

consequently a shift in the temperature distribution towards the inlet temperature. Moreover, the tangential temperature gradients in this region are negative at lower wall.
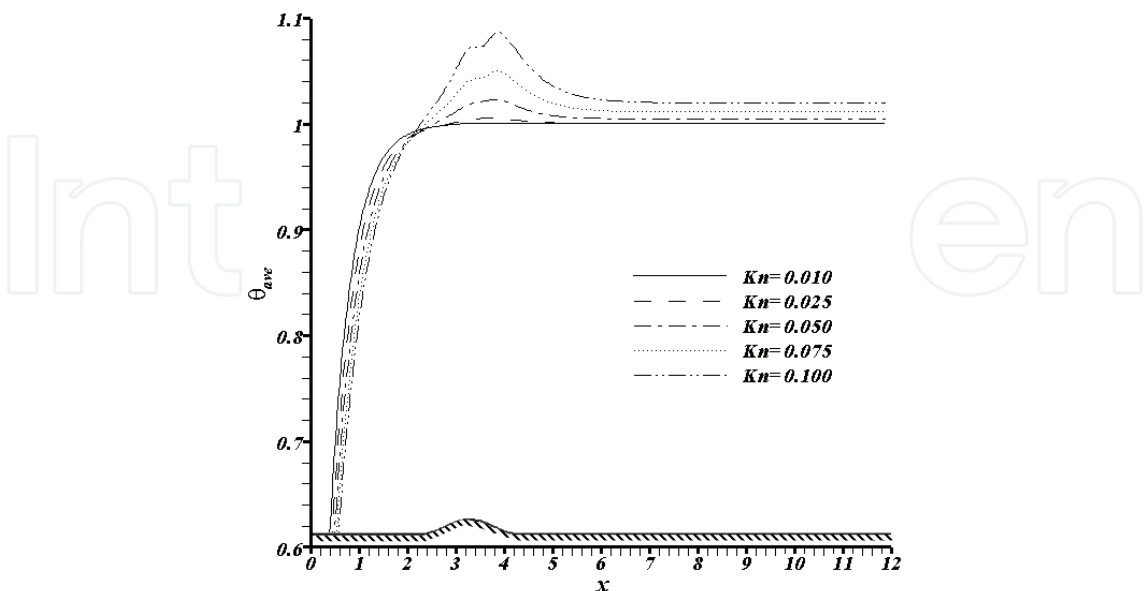

Fig. 12. Variation of average temperature with Knudsen number along the constricted microchannel at Re=2 and a=0.15
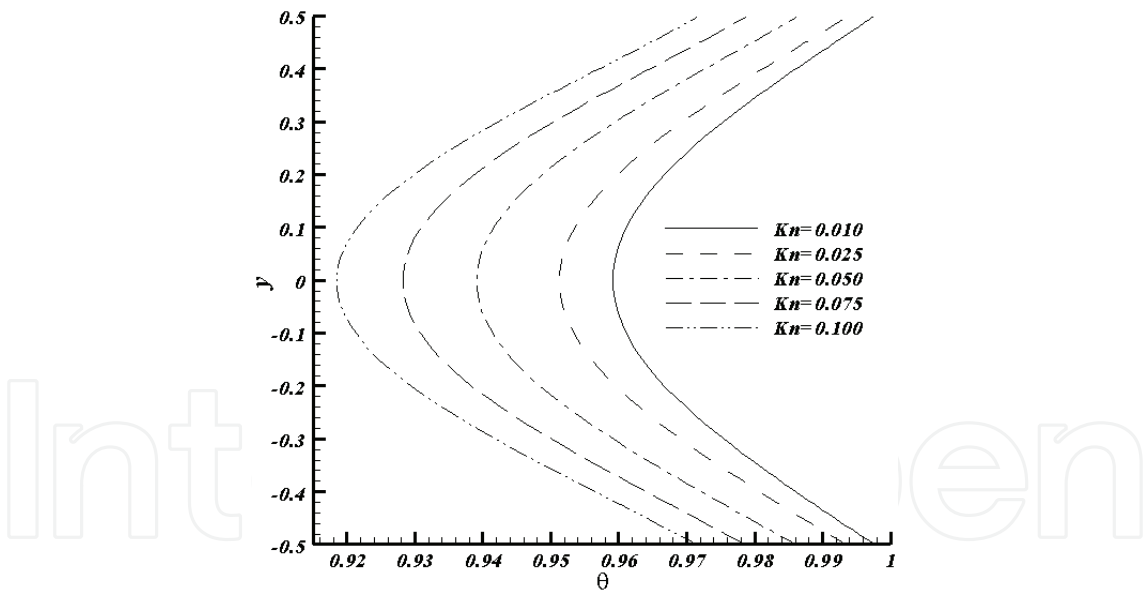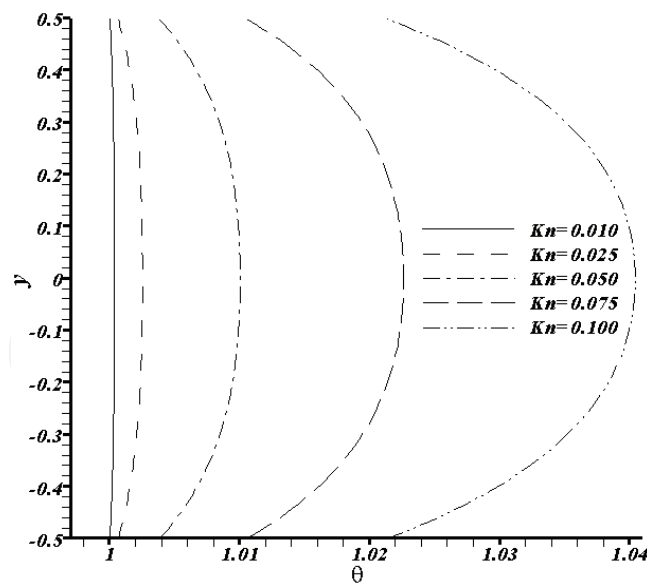

Fig. 13. Variation of temperature profile at x=0.75λ in the constricted microchannel with Knudsen number at Re=2 and a=0.15

In Fig. 14, the temperature profiles are located in the region of θ>1 (the outlet region with higher viscous dissipation effects). As mentioned above, in this region the increasing effect of Knudsen number on temperature jump is in different direction. As Knudsen number increases, the temperature distribution shifts towards higher temperatures. In addition, in this region tangential temperature gradients at lower wall are positive and also are larger with higher Knudsen numbers.

Fig. 14. Variation of temperature profile at x=2.5λ in the constricted microchannel with Knudsen number at Re=2 and a=0.15

The effect of Knudsen number on local Nusselt number is depicted in Fig. 15. As observed, due to high temperature gradients in the entrance of microchannel, local Nusselt number has great value in this region. However this high heat transfer rates diminish rapidly as the flow develops thermally. After the entrance region and before the constricted part, a singular point is observed at each Knudsen number where the value of Nusselt number goes to infinity. However, the Nusselt number goes to infinity, it does not mean that there is infinite heat transfer in this point at all. The physical reason is that at this point the average temperature and wall temperature have locally the same value and their difference vanishes. In other word, at this point the heat supplied by the walls equals the heat generated by viscous dissipation effect and there is no net heat transfer at this point between the wall and the adjacent fluid. By increasing the Knudsen number and consequently increasing the viscous dissipation effect, this singular point occurs at closer distances to the entrance of channel. This effect also was observed in Fig. 10 where by increasing Knudsen number, the region of θ>1 grows. Furthermore, the Nusselt number is positive before and after the singular point. According to Eq. (32), two different parameters determine the sign of Nusselt number, the tangential temperature gradient and the difference of average nondimensional temperature and wall temperature. In the region of θ<1 (i.e. the region before the singular point) the difference of average nondimensional temperature and wall temperature is negative and according to Fig. 13, the tangential temperature gradient is also negative. So Nusselt number is positive. On the contrary, in the region of θ>1, these two parameters are positive that leads to positive Nusselt number again.

Moreover, by increasing Knudsen number, Nusselt number decreases. For instance, by variation of Knudsen number from 0.01 to 0.1, developed Nusselt number decreases 57%. To explain this phenomenon, one should pay attention to two parameters, the temperature jump and slip velocity. As already stated, the temperature jump and slip velocity increase with Knudsen number. Here, the temperature jump means the absolute difference between the average temperature and wall temperature. So temperature jumps acts like a thermal contact resistance between the wall and gas. On the other side, the slip velocity tends to decrease this contact resistance. So these parameters tend to affect Nusselt number in different direction. As the slip velocity increases the Nusselt number by increasing the fluid

velocity near wall, the temperature jump decreases the Nusselt number by increasing the absolute difference of the wall temperature and mean gas temperature. In this work, by choosing σ_v=0.9, σ_T=0.9 and the specified geometry, it is observed that the effect of temperature jump is dominant.

Furthermore, in the convergent region, due to increasing of the average velocity and especially slip velocity, there is a jump in local Nusselt number. As the fluid flow approaches the developed region, no change in local Nusselt number is observed and local Nusselt number converges to its fully developed value.
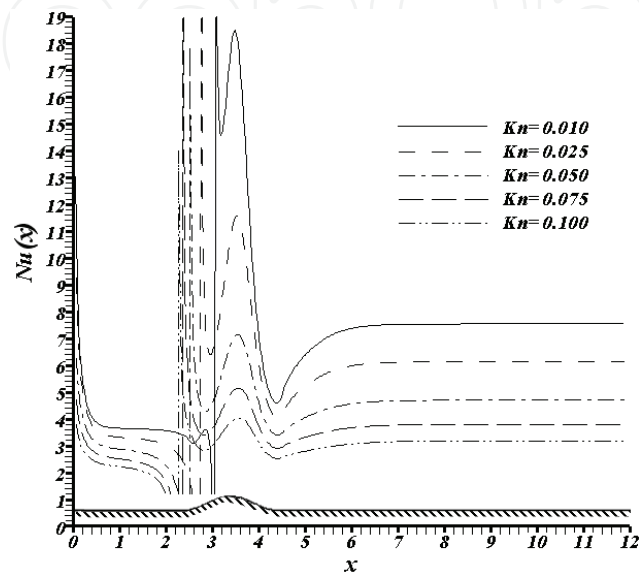
Fig. 15. Variation of local Nusselt number along the constricted microchannel with Knudsen number at Re=2 and a=0.15
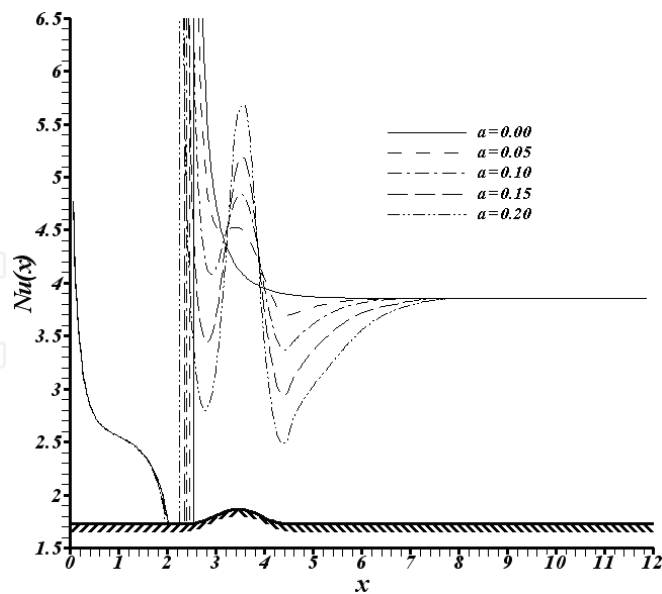
Fig. 16. Variation of local Nusselt number along the constricted microchannel with ampilitude of the wave at Kn=0.075 and Re=2

Fig. 16 illustrates the variation of Nusselt number as a function of amplitude of the wave, while keeping the Reynolds number and Knudsen number constant. The effect of

constriction on Nusselt number is more sensible for lesser throttle area. In other word, by decreasing the throttle area and consequently increasing the average velocity, Nusselt number experiences much larger jump. For instance, by variation of amplitude of the wave from 0.05 to 0.15, Nusselt number increases 15% in the throttle region.
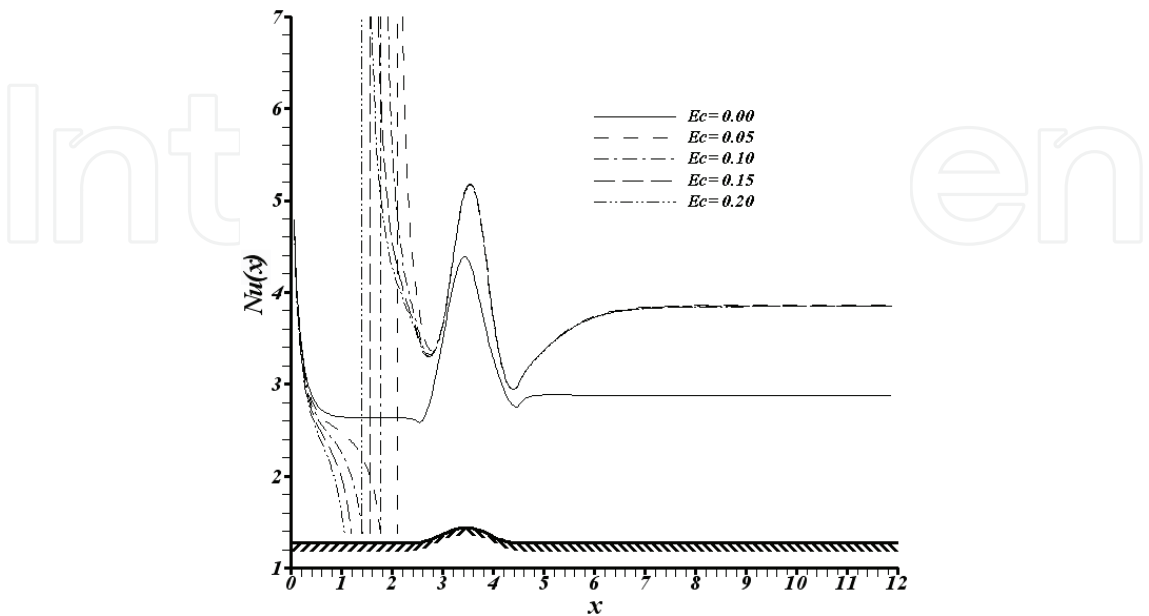

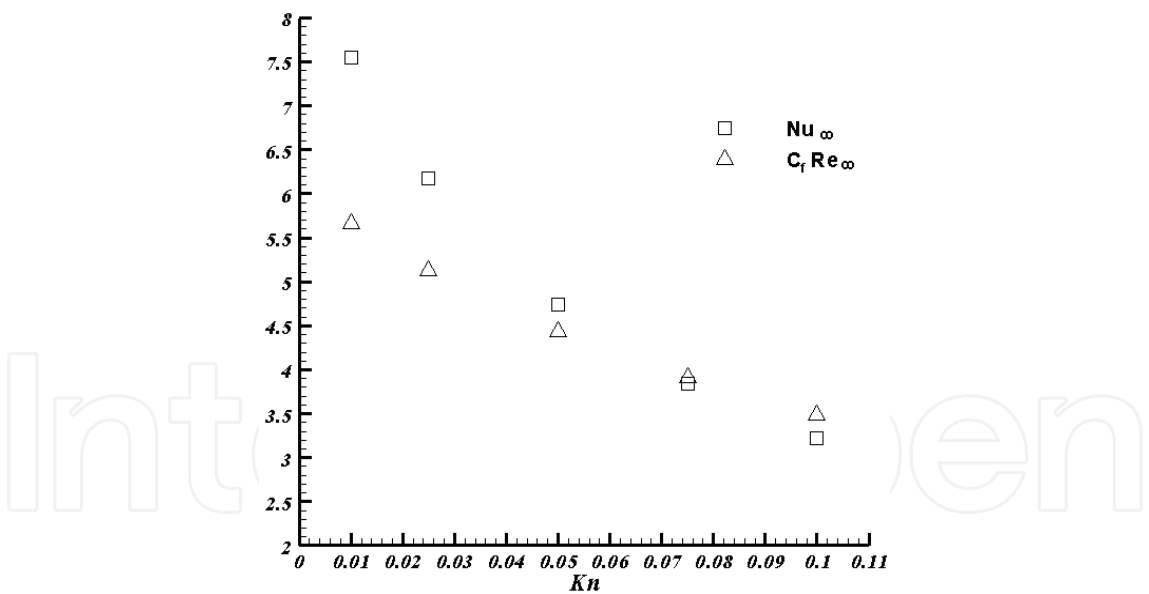Fig. 17. Variation of local Nusselt number with Eckert number at Re=2, Kn=0.075 and a=0.15

Fig. 18. Variation of developed $C_f.Re$ and Nusselt number with Knudsen number at Re=2 and a=0.15

A comparison is carried out in Fig. 17 to investigate the effect of viscous dissipation on local Nusselt number. As already stated, viscous dissipation cause a singular point in local Nusselt number. In addition, taking viscous dissipation into account causes an increase in Nusselt number. Viscous dissipation increases the average temperature and accordingly in the region of $\theta > 1$ increases the difference of average temperature and wall temperature. Therefore, the heat transfer rate in this region is enhanced. Also, in Eq. (11), wall

temperature gradient increases by involving viscous dissipation and this increase is dominant. Therefore, it causes the Nusselt number to increase. Furthermore, as it is depicted, by increasing the Eckert number from 0.05 to 0.2, the fully developed Nusselt number does not vary, but the location of singular point changes. In Fact, as Eckert number increases, the viscous dissipation effect and consequently the region of $\theta > 1$ increases and the singular point occurs at closer distances to the entrance of channel.

In Fig. 18, the developed Nusselt number and $C_f.Re$ at the end of constricted microchannel verses Knudsen number are reported. The decreasing effect of Knudsen number on developed Nusselt number and $C_f.Re$ is obvious in this figure. Moreover, by variation of Knudsen number from 0.01 to 0.1, the Nu_∞ and $C_f.Re_\infty$ declines 57% and 38% respectively.

8. Conclusion

The thermally/ hydrodynamically fluid flow through a constricted microchannel is studied by taking the effect of viscous dissipation into account. The numerical method which was served to solve governing equations is a finite volume method (SIMPLE) in curvilinear coordinate. In this study, effects of Knudsen number and geometry on $C_f.Re$ and Nusselt number are investigated. The results show that viscous dissipation significantly affects the thermal behavior of fluid flow. However, hydrodynamic flow field is slightly affected by viscous dissipation.

The main results obtained can be summarized as follows:

4. The rarefaction effect intensifies the temperature jump and slip velocity at the solid walls.
5. By increasing the Knudsen number, Nusselt number and $C_f.Re$ decrease. For instance, Nusselt number and $C_f.Re$ decrease 57% and 38% respectively at the end of the microchannel in the range of $0.01 < Kn < 0.1$.
6. Convergent region makes $C_f.Re$ to decrease rapidly and amplitude of wave intensifies this decrease.
7. Nusselt number experiences a rapid jump in the convergent part and this jump is more considerable for lower Knudsen numbers and higher amplitude of wave.
8. The effect of viscous dissipation is more significant by increasing Knudsen number. Also, viscous dissipation leads a singular point in Nusselt number profiles.
9. Viscous dissipation increases local Nusselt number. However, it does not significantly affect $C_f.Re$.

9. References

[1] L. M. Jiji, 2008, "Effect of Rarefaction, Dissipation, and Accommodation Coefficients on Heat Transfer in Microcylindrical Couette Flow," ASME J. Heat Transfer, 130, pp. 385-393.

[2] I. A. Graur, J. G. Me´olans, D. E. Zeitoun, 2006, "Analytical and numerical description for isothermal gas flows in microchannels," Microfluid Nanofluid, 2, pp. 64-67.

[3] E. Galvis, B. A. Jubran, F. Xi, K. Behdinan, Z. Fawaz, 2008, "Numerical modeling of pin–fin micro heat exchangers," Heat Mass Transfer, 44, pp. 659–666.

[4] D. Jie, X. Diao, K. B. Cheong, L. K. Yong, 2000, "Navier–Stokes simulations of gas flow in micro devices," J. Micromech. Microeng, 10, pp. 372–379.

[5] L. Biswal, S.K. Som, S. Chakraborty, "Effects of entrance region transport processes on free convection slip flow in vertical microchannels with isothermally heated walls, International Journal of Heat and Mass Transfer 50 (2007) 1248–1254.

[6]   G. Hetsroni, A. Mosyak, E. Pogrebnyak, L.P. Yarin, Fluid flow in micro-channels, International Journal of Heat & Mass Transfer 48 (2005) 1982–1998.

[7]   A. Beskok, G.E. Karniadakis, Simulation of heat and momentum transfer in complex microgeometries, J. Thermophys Heat Transfer 8 (1994) 647–655.

[8]   R. T-S. Cheng, 1972, "Numerical Solution of the Navier-Stokes Equations by the Finite Element Method," Phys. Fluids, 15, pp. 2098–2105.

[9]   J. E. O'Brien and E. M. Sparrow, Corrugated-duct heat transfer, pressure drop, and flow visualization, J. Heat Transfer 104 (1982) 410-416.

[10] T. Nishimura, Y. Ohori, Y. Kawamura, 1984, "Flow characteristics in a channel with symmetric wavy wall for steady flow," J. Chem. Eng. Jpn., 17, pp. 466-471.

[11] C. C. Wang, C. K. Chen, 2002, "Forced convection in a wavy-wall channel," International Journal of Heat and Mass Transfer, 45, pp. 2587-2595.

[12] E. B. Arkilic, K. S. Breuer, M. A. Schmidt, 1994, "Gaseous Flow in Microchannels," ASME Application of Microfabrication to Fluid Mechanics, 197, pp. 57–66.

[13] A. Beskok, G. E. Karniadakis, Trimmer, W., 1996, "Rarefaction and compressibility effects in gas microflows," ASME Journal of Fluids Engineering, 118, pp. 448-456.

[14] L. Kuddusi, E. Çetegen, Thermal and hydrodyna-mic analysis of gaseous flow in trapezoidal silicon microchannels, International Journal of Thermal Sciences 48 (2009) 353–362.

[15] Cha'o-Kuang Chen, Ching-Chang Cho, Electro-kinetically-driven flow mixing in microchannels with wavy surface, Journal of Colloid and Interface Science 312 (2007) 470–480.

[16] H. Shokouhmand, S. Bigham, Slip-flow and heat transfer of gaseous flows in the entrance of a wavy microchannel, International Communications in Heat and Mass Transfer 37 (2010) 695–702.

[17] Hossein Shokouhmand, Sajjad Bigham, Rasool Nasr Isfahani, Effects of Knudsen number and geometry on gaseous flow and heat transfer in a constricted microchannel, Heat Mass Transfer (2011) 47:119–130.

[18] Sajjad Bigham, Hossein Shokouhmand, Rasool Nasr Isfahani, and Sajjad Yazdani, FLUID FLOW AND HEAT TRANSFER SIMULATION IN A CONSTRICTED MICROCHANNEL: EFFECTS OF RAREFACTION, GEOMETRY, AND VISCOUS DISSIPATION, Numerical Heat Transfer, Part A, 59: 209–230, 2011.

[19] K. A. Hoffman, 1989, Computational fluid dynamics for engineers, Engineering Education System, Austin.

[20] E. H. Kennard, 1938, Kinetic theory of gasses, McGraw-Hill, New York.

[21] G. E. Karniadakis, A. Beskok, N. Aluru, 2004, Micro Flows and Nanoflows, Fundamental and Simulation, Springer, USA.

[22] S. Kandlikar, S. Garimella, D. Li, S. Colin, M. R. King, 2006, Heat Transfer And Fluid Flow In Minichannels and Microchannels, Elsevier, Britain.

[23] W. W. Liou, Y. Fang, Microfluid Mechanics, 2006, Principal and Modeling, McGraw-Hill, New York.

[24] S. V. Patankar, 1972, A calculation procedure for heat, mass and momentum transfer in three-dimensional parabolic flows, Int J. Heat Mass Transf., 15, pp. 1787–1806.

[25] D. B. Spalding, 1972, "A novel finite difference formulation for differential expressions involving both first and second derivatives", Int J Numer Methods Eng, 4, pp. 551-559.

[26] J. V. Rij, T. Ameel, T. Harman, 2009, "The effect of viscous dissipation and rarefaction on rectangular microchannel convective heat transfer," International Journal of Thermal Sciences, 48, pp. 271–281.
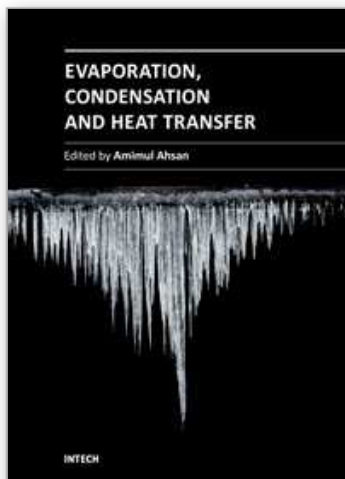
Evaporation, Condensation and Heat transfer

Edited by Dr. Amimul Ahsan

The theoretical analysis and modeling of heat and mass transfer rates produced in evaporation and condensation processes are significant issues in a design of wide range of industrial processes and devices. This book includes 25 advanced and revised contributions, and it covers mainly (1) evaporation and boiling, (2) condensation and cooling, (3) heat transfer and exchanger, and (4) fluid and flow. The readers of this book will appreciate the current issues of modeling on evaporation, water vapor condensation, heat transfer and exchanger, and on fluid flow in different aspects. The approaches would be applicable in various industrial purposes as well. The advanced idea and information described here will be fruitful for the readers to find a sustainable solution in an industrialized society.

How to reference

In order to correctly reference this scholarly work, feel free to copy and paste the following:

INTECH
open science | open minds